

Enhanced sensing of optomechanically induced nonlinearity by linewidth suppression and optical bistability in cavity-waveguide systems

Chun-Wang Liu, Ye Liu, Wan-Jun Su, and Huaizhi Wu

Fujian Key Laboratory of Quantum Information and Quantum Optics and Department of Physics, Fuzhou University, Fuzhou 350116, People's Republic of China

Lei Du

Center for Quantum Sciences and School of Physics, Northeast Normal University, Changchun 130024, China

Yong Li

Center for Theoretical Physics and School of Science, Hainan University, Haikou 570228, China and Synergetic Innovation Center for Quantum Effects and Applications, Hunan Normal University, Changsha 410081, China

We study enhanced sensing of optomechanically induced nonlinearity (OMIN) in a cavity-waveguide coupled system. The Hamiltonian of the system is anti-PT symmetric with the two involved cavities being dissipatively coupled via the waveguide. When a weak waveguide-mediated coherent coupling is introduced, the anti-PT symmetry may break down. However, we find a strong bistable response of the cavity intensity to the OMIN near the cavity resonance, benefiting from linewidth suppression caused by the vacuum induced coherence. The joint effect of optical bistability and the linewidth suppression is inaccessible by the anti-PT symmetric system involving only dissipative coupling. Due to that, the sensitivity is greatly enhanced by two orders of magnitude compared to that for the anti-PT symmetric model. Moreover, the sensitivity shows resistances to a reasonably large cavity decay and robustness to fluctuations in the cavity-waveguide detuning. Based on the integrated optomechanical cavity-waveguide systems, the scheme can be used for sensing different physical quantities related to the single-photon coupling strength, and has potential applications in high-precision measurements with physical systems involving Kerr-type nonlinearity.

I. INTRODUCTION

Sensing has played an important role in cutting-edge technologies, associated with the-state-of-the-art metrology platforms for measurements of various physical quantities [1], ranging from magnetic and electric fields [2, 3], to time and frequency [4], to minute force [5], acceleration [6], and mass [7, 8]. In contrast to the conventional Hermitian systems, where the sensing of weak perturbations hinges on the linear response of resonant spectrum shifts or splitting to a perturbation parameter, recent advances have found that a new type of sensing schemes can be built on the non-Hermitian Hamiltonians with Parity-Time (PT) [9–12] or anti-PT symmetry [13–18]. The spectra for such a kind of non-Hermitian Hamiltonians typically exhibit exceptional point (EP) singularities, at which the eigenvalues and the corresponding eigenvectors coalesce [8, 19–22]. As a result, an external perturbation on the system parameter across the EPs leads to phase transitions between the PT (anti-PT) phase with a purely real (imaginary) spectra and the broken PT (anti-PT) phase with complex eigenvalues. Moreover, the response to linear perturbations shows a power-law divergence behavior in the first-order derivative with respect to the perturbation parameter [14], which makes the PT and anti-PT symmetric systems the good candidates for sensitivity enhancement [17, 23–25]. The EP physics has been experimentally demonstrated in different settings for real-

izing nonreciprocal light transport [26, 27], single-mode lasers [28, 29], time-asymmetric topological operations [30, 31], enhanced sensing [10, 20, 32, 33], as well as energy-difference conserving dynamics [34].

While early EP studies have focused on sensing linear perturbations with non-Hermitian systems [17], recent attentions have been paid to the detection of anharmonic perturbations, which are essential for quantum state engineering and creation of non-Gaussian bosonic fields. As an example, Nair *et al.* have recently proposed an anti-PT symmetry sensing enhancement scheme in the context of a weakly anharmonic yttrium iron garnet sphere interacting with a cavity via a fiber waveguide in the vacuum [18]. In contrast to the gain-loss balanced system in the PT symmetric phase [10–12], which has purely real eigenvalues, the system in the anti-PT symmetric phase may have a unique singular point corresponding to the emergence of only one real eigenvalue, which is referred to as the linewidth suppression caused by the vacuum induced coherence (VIC) [35–40]. It was shown that the nonlinear response of the cavity intensity around the singularity can efficiently quantify the strength of the anharmonicity explicitly included in the Kittel mode of spins [41]. Besides the cavity-magnonics [24], many other physical settings, which have been tailored to exhibit anti-PT symmetry [42–45] and to sense linear perturbations [15, 17, 46], may have potentials to detect fundamental nonlinear oscillators, manifesting themselves in many modern fields of physics, e.g., quantum electrical circuits [47], cold atoms [48], levi-

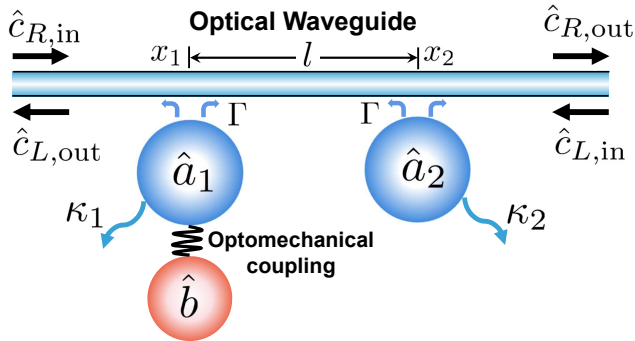


Figure 1. (Color online) Schematic of the optomechanical cavity-waveguide system. A cavity optomechanical system (consisting of an optical mode \hat{a}_1 and a mechanical mode \hat{b}) is coupled to the auxiliary cavity mode \hat{a}_2 through an optical waveguide with a linear dispersion relation. $\hat{c}_{L,\text{in}}(x_j, t)$ and $\hat{c}_{R,\text{in}}(x_j, t)$ denote the left- and right-moving fields which interact with the cavity modes at the position x_j with the strength Γ . The cavity modes \hat{a}_j decay into the surrounding environments with the rates κ_j .

tated nanoparticles [49, 50], and optomechanical systems [51, 52]

In this paper, we study enhanced sensing of optomechanical interactions with a coupled cavity-waveguide system. The system consists of an optomechanical cavity and an auxiliary cavity, which are coupled via a one-dimensional waveguide in the vacuum. The Hamiltonian of the system can be anti-PT symmetric if the two cavities are dissipatively coupled, which is valid only when the phase accumulation of light propagation from one cavity to the other is precisely a multiple of 2π . When a phase deviation is introduced, a coherent coupling between the cavity modes is induced and the anti-PT symmetry can not hold. Then, there does not exist the eigenvalue with vanishing imaginary part, and the eigenmodes are subject to a finite loss to the waveguide, which may be detrimental to sensing of anharmonicity in the cavity modes [18]. On the other hand, it is well known that optical bistability can appear in the presence of a Kerr nonlinearity with appropriate cavity drivings. However, the standard anti-PT symmetric system shows bistability only when the frequency detuning between the cavity modes is large enough. This condition is related to the broken anti-PT phase, where the VIC induced linewidth suppression can not be found [53]. Here, by considering the optomechanically induced Kerr-type nonlinearity and introducing a phase deviation to the field propagation, we find that optical bistability can occur at the cavity resonance, where the system Hamiltonian does not have the purely real eigenvalue, but the VIC induced linewidth suppression still holds, corresponding to a long-lived eigenmode. By combining the advantages of the resonant linewidth suppression and the optical bistability, a strong bistable response of the cavity intensity to the OMIN can be found. By comparing the

responses to two optomechanical strengths with a factor of 3 difference, we identify two working regions for sensing of the OMIN. In the first region, the system may display monostability (or optical bistability) for both coupling strengths, where the sensitivity can be double compared to that of the anti-PT symmetric model. In the second region, the system displays monostable behavior for one strength and optical bistability for the other, then a remarkably high sensitivity of a few hundreds can be achieved. Moreover, the sensing scheme is resistant to a weak cavity decay, and effectively functions with the sensitivity remaining a few tens. As an example, we envision a cascaded optomechanical setup where an optically levitated nanodiamond couples to two waveguide-coupled microspheres [54]. The model can be potentially generalized to other integrated optomechanical cavity-waveguide systems, such as hybrid cavity-magnonic systems [55, 56], optical crystal circuits [57], and microwave optomechanical circuits [58].

The remainder of the paper is organized as follows. In Sec. II, we first derive the coherent and dissipative couplings between two optical cavities coupled via a vacuum waveguide. In Sec. III, we recall the anti-PT symmetric system constructed by the coupled cavity-waveguide setup, and discuss the VIC induced linewidth suppression significantly for sensing of the OMIN. In Sec. IV, we examine the coherence induced bistability around the cavity resonance, based on which, the sensitivity enhancement can be realized, as studied in Sec. V. We discuss the experimental feasibility of the scheme in Sec. VI and summarized our results in Sec. VII.

II. THEORETICAL MODEL

As schematically shown in Fig. 1, we start by considering the general model where two cavity modes \hat{a}_1 and \hat{a}_2 of frequencies ω_1 and ω_2 , respectively, are coupled via a waveguide, and have the decays rates κ_1 and κ_2 . The cavity mode \hat{a}_1 is coupled to a mechanical mode of the frequency ω_m via the standard optomechanical interaction. For simplicity, we assume that the waveguide has a linear dispersion relation $\omega(k) = v_G|k|$ for the left- and right-going waveguide modes of wavevector k . Working at the rotating frame with respect to the central frequency $\omega_0 \equiv (\omega_1 + \omega_2)/2$ of the two coupled cavities, the Hamiltonian of the system is then given by ($\hbar = 1$) [59–62]

$$H = H_C + H_W + H_{CW} \quad (1)$$

with

$$H_C = \frac{\delta}{2} (\hat{a}_1^\dagger \hat{a}_1 - \hat{a}_2^\dagger \hat{a}_2) + \frac{\omega_m}{2} (\hat{p}^2 + \hat{q}^2) + g \hat{a}_1^\dagger \hat{a}_1 \hat{q} + i \Omega \hat{a}_1^\dagger e^{-i(\omega_d - \omega_0)t} + \text{H.c.}, \quad (2)$$

$$H_W = \int dx [\hat{c}_R^\dagger(x) (-iv_G \frac{\partial}{\partial x} - \omega_0) \hat{c}_R(x)$$

$$+\hat{c}_L^\dagger(x)(iv_G\frac{\partial}{\partial x}-\omega_0)\hat{c}_L(x)], \quad (3)$$

$$H_{CW} = -\sqrt{\frac{\Gamma v_G}{2}} \sum_{j=1,2} \hat{a}_j^\dagger [\hat{c}_R(x_j) + \hat{c}_L(x_j)] + \text{H.c.}, \quad (4)$$

where H_C describes the interaction of the cavity mode with the mechanical motion via the radiation pressure force with \hat{q} (\hat{p}) being the mechanical displacement (momentum) operator, and g being the single-photon optomechanical coupling strength. The cavity mode a_1 is driven by an external laser field of the amplitude $\Omega = \sqrt{P_{\text{in}}\kappa_1/\hbar\omega_d}$ with P_{in} being the input power and ω_d the laser frequency, which is set to $\omega_d = \omega_0$ in what follows. $\hat{c}_{L,R}(x_j)$ denote the left- and right-going modes in the waveguide, which couple to cavity j at position x_j with the rate Γ [59].

The optical cavities can be dissipatively coupled by reservoir engineering the waveguide field, and can be further designed as an anti-PT symmetric system [18]. To see this, we first leave the optomechanical interaction out and include it later as the probe. Then, the Heisenberg equations of motion for the waveguide modes are given by [60]

$$\begin{aligned} \frac{\partial}{\partial t} \hat{c}_R(x, t) &= (-v_G \frac{\partial}{\partial x} + i\omega_0) \hat{c}_R(x, t) \\ &+ i \sum_{j=1,2} \sqrt{\frac{\Gamma v_G}{2}} \delta(x - x_j) \hat{a}_j, \end{aligned} \quad (5)$$

$$\begin{aligned} \frac{\partial}{\partial t} \hat{c}_L(x, t) &= (v_G \frac{\partial}{\partial x} + i\omega_0) \hat{c}_L(x, t) \\ &+ i \sum_{j=1,2} \sqrt{\frac{\Gamma v_G}{2}} \delta(x - x_j) \hat{a}_j. \end{aligned} \quad (6)$$

By integrating the field equations across the discontinuity at x_j , one obtains the input-output relations between the cavity modes and the left- (right-) going fields [60]

$$\hat{c}_R(x_j^+, t) - \hat{c}_R(x_j^-, t) = i\sqrt{\frac{\Gamma}{2v_G}} \hat{a}_j(t), \quad (7)$$

$$\hat{c}_L(x_j^-, t) - \hat{c}_L(x_j^+, t) = i\sqrt{\frac{\Gamma}{2v_G}} \hat{a}_j(t). \quad (8)$$

For clarity, we can further define $\hat{c}_{L,\text{in}}(x_j, t) \equiv \hat{c}_L(x_j^+, t)$ and $\hat{c}_{R,\text{in}}(x_j, t) \equiv \hat{c}_R(x_j^-, t)$ as the input fields to the cavities from the waveguide, and $\hat{c}_{L,\text{out}}(x_j, t) \equiv \hat{c}_L(x_j^-, t)$ and $\hat{c}_{R,\text{out}}(x_j, t) \equiv \hat{c}_R(x_j^+, t)$ as the output fields. This leads to the familiar form of the standard input-output relations:

$$\begin{aligned} \hat{c}_{R,\text{out}}(x_j, t) &= \hat{c}_{R,\text{in}}(x_j, t) + i\sqrt{\frac{\Gamma}{2v_G}} \hat{a}_j, \\ \hat{c}_{L,\text{out}}(x_j, t) &= \hat{c}_{L,\text{in}}(x_j, t) + i\sqrt{\frac{\Gamma}{2v_G}} \hat{a}_j. \end{aligned} \quad (9)$$

In addition, since the waveguide field propagates freely between the cavities and the waveguide dispersion is linear over all frequencies, we have [59, 63, 64]

$$\begin{aligned} \hat{c}_{R,\text{in}}(x_2, t) &= e^{i\Phi} \hat{c}_{R,\text{out}}(x_1, t), \\ \hat{c}_{L,\text{in}}(x_1, t) &= e^{i\Phi} \hat{c}_{L,\text{out}}(x_2, t), \end{aligned} \quad (10)$$

where $\Phi = kl$ with $l \equiv |x_2 - x_1|$. Consider the case where for the frequencies of interest around ω_0 , the phase delay $\delta(l/v_G) \ll 1$ due to field propagation is ignorable, we can then replace k by $k_0 \equiv \omega_0/v_G$ [59]. Moreover, we are concerned with the Markovian approximation $\kappa(l/v_G) \ll 1$, and thus the retarded effect on the cavity dynamics due to the field propagation can also be neglected. Based on these assumptions, one can achieve the Φ -dependent coupling between the two cavities. To see this, we further write down the Heisenberg equations of motion for the cavity operators without the optomechanical coupling,

$$\begin{aligned} \dot{\hat{a}}_1 &= -\left(-i\frac{\delta}{2} + \frac{\kappa_1}{2}\right) \hat{a}_1 + \Omega + \sqrt{\kappa_1} \hat{a}_{1,\text{in}} \\ &+ i\sqrt{\frac{\Gamma v_G}{2}} [\hat{c}_{R,\text{out}}(x_1, t) + \hat{c}_{L,\text{in}}(x_1, t)], \end{aligned} \quad (11)$$

$$\begin{aligned} \dot{\hat{a}}_2 &= -\left(i\frac{\delta}{2} + \frac{\kappa_2}{2}\right) \hat{a}_2 + \sqrt{\kappa_2} \hat{a}_{2,\text{in}} \\ &+ i\sqrt{\frac{\Gamma v_G}{2}} [\hat{c}_{R,\text{out}}(x_2, t) + \hat{c}_{L,\text{in}}(x_2, t)], \end{aligned} \quad (12)$$

and substitute Eqs. (9) and (10) into Eqs. (11) and (12). It then follows that

$$\begin{aligned} \dot{\hat{a}}_1 &= -\left(-i\frac{\delta}{2} + \frac{\kappa_1 + \Gamma}{2}\right) \hat{a}_1 - ie^{i\Phi} \frac{\Gamma}{2} \hat{a}_2 + \Omega + \sqrt{\kappa} \hat{a}_{1,\text{in}} \\ &+ i\sqrt{\frac{\Gamma v_G}{2}} [\hat{c}_{R,\text{in}}(x_1, t) + e^{i\Phi} \hat{c}_{L,\text{in}}(x_2, t)], \end{aligned} \quad (13)$$

$$\begin{aligned} \dot{\hat{a}}_2 &= -\left(i\frac{\delta}{2} + \frac{\kappa_2 + \Gamma}{2}\right) \hat{a}_2 - ie^{i\Phi} \frac{\Gamma}{2} \hat{a}_1 + \sqrt{\kappa} \hat{a}_{2,\text{in}} \\ &+ i\sqrt{\frac{\Gamma v_G}{2}} [e^{i\Phi} \hat{c}_{R,\text{in}}(x_1, t) + \hat{c}_{L,\text{in}}(x_2, t)], \end{aligned} \quad (14)$$

where $\hat{a}_{j,\text{in}}$ ($j = 1, 2$) are zero-mean quantum noises and the cavity decay rates $\kappa_1 = \kappa_2 = \kappa$ are assumed to be identical. The above equations can be rewritten in the matrix form

$$\begin{pmatrix} \dot{\hat{a}}_1 \\ \dot{\hat{a}}_2 \end{pmatrix} = -i\mathcal{H} \begin{pmatrix} \hat{a}_1 \\ \hat{a}_2 \end{pmatrix} + \begin{pmatrix} \Omega + \hat{a}_{1,N} \\ \hat{a}_{2,N} \end{pmatrix}, \quad (15)$$

with

$$\mathcal{H} = \begin{pmatrix} -\frac{\delta}{2} - i\frac{\kappa+\Gamma}{2} & -i\frac{\Gamma}{2} \cos\Phi + \frac{\Gamma}{2} \sin\Phi \\ -i\frac{\Gamma}{2} \cos\Phi + \frac{\Gamma}{2} \sin\Phi & \frac{\delta}{2} - i\frac{\kappa+\Gamma}{2} \end{pmatrix} \quad (16)$$

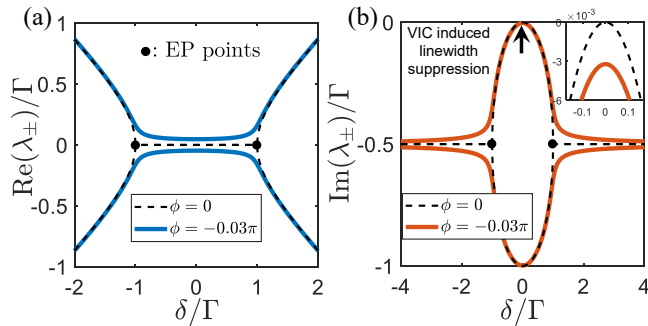


Figure 2. (Color online) (a) Real parts (eigenfrequencies) and (b) imaginary parts (linewidths) of the eigenvalues of \mathcal{H} versus the detuning δ/Γ for $\phi = 0$ (dashed) and $\phi = -0.03\pi$ (solid), respectively. The cavity decay rates are set to zero such that the VIC induced zero linewidth ($\text{Im}\lambda_+/\Gamma = 0$) arises at the resonance ($\delta = 0$) for the anti-PT symmetric regime $\phi = 0$. The EPs disappear for $\phi \neq 0$, but the VIC induced linewidth suppression (with $\text{Im}\lambda_+/\Gamma \rightarrow 10^{-3}$) remains effective for $\delta \rightarrow 0$ and $\phi \ll \pi$, as can be seen from the inset. Here, we consider a finite cavity linewidth with $\kappa/\Gamma = 0.002$.

and the total input noise operators being defined as

$$\begin{aligned} \hat{a}_{1,N} &= \sqrt{\kappa} \hat{a}_{1,\text{in}} + i\sqrt{\frac{\Gamma v_G}{2}} [\hat{c}_{R,\text{in}}(x_1, t) + e^{i\Phi} \hat{c}_{L,\text{in}}(x_2, t)], \\ \hat{a}_{2,N} &= \sqrt{\kappa} \hat{a}_{2,\text{in}} + i\sqrt{\frac{\Gamma v_G}{2}} [e^{i\Phi} \hat{c}_{R,\text{in}}(x_1, t) + \hat{c}_{L,\text{in}}(x_2, t)], \end{aligned} \quad (17)$$

which have the zero mean for $\hat{c}_{L,\text{in}}(x_1, t)$ and $\hat{c}_{R,\text{in}}(x_1, t)$ being the Gaussian white noises as well [59]. Note that, the waveguide acts as an engineered reservoir, which induces coherent and dissipative couplings between the two optical modes with amplitudes $(\Gamma/2)\sin\Phi$ and $(\Gamma/2)\cos\Phi$, respectively. The model, under the anti-PT symmetric case (i.e. $e^{i\Phi} = \pm 1$), has been applied for sensing weak anharmonicities in a yttrium iron garnet sphere interacting with a cavity-fiber system [18]. Instead of placing a Kerr interaction term in the Hamiltonian, here in our case, the optomechanical interaction with the single-photon coupling strength g is included. A Kerr-type nonlinearity proportional to g^2 in the optomechanical cavity will be generated when the system is in the steady state, see details in the following section. We then focus on the enhanced sensing of weak optomechanical interactions by using the coupled cavity-waveguide system with a finite coherent coupling (i.e. $e^{i\Phi} \neq \pm 1$), which can be efficient for measurement of the physical quantities related to the optomechanical single-photon coupling strength g .

III. THE VIC INDUCED LINEWIDTH SUPPRESSION

For the propagating phase being a multiple of 2π , i.e. $\Phi = 2n\pi$ ($n \in \mathbb{Z}$), the coherent coupling with the amplitude $(\Gamma/2)\sin\Phi$ between the cavity modes vanishes [59], leading to a purely dissipative hopping interaction of the strength $\Gamma/2$. The matrix \mathcal{H} reduces to the standard anti-PT symmetric form

$$\mathcal{H}_{APT} = \begin{pmatrix} -\frac{\delta}{2} - i\frac{\kappa+\Gamma}{2} & -i\frac{\Gamma}{2} \\ -i\frac{\Gamma}{2} & \frac{\delta}{2} - i\frac{\kappa+\Gamma}{2} \end{pmatrix}, \quad (18)$$

where the two coupled cavity modes have: (i) opposite frequency detunings and the same gain or loss; and (ii) dissipative coupling (anti-Hermitian coupling) between them. Thus, the Hamiltonian obeys $(\widehat{PT})\mathcal{H}_{APT}(\widehat{PT}) = -\mathcal{H}_{APT}$ and is anti-PT symmetric [18, 24]. One can readily obtain the eigenvalues of \mathcal{H}_{APT} ,

$$\lambda_{\pm} = -i\frac{\kappa+\Gamma}{2} \pm \frac{1}{2}\sqrt{\delta^2 - \Gamma^2}, \quad (19)$$

which are plotted against δ/Γ , as shown in Fig. 2. In the anti-PT symmetric phase $|\delta/\Gamma| < 1$, \mathcal{H}_{APT} has purely imaginary eigenvalues $\lambda_{\pm} = -i\frac{\kappa+\Gamma}{2} \pm i\frac{1}{2}\lambda_0$ with $\lambda_0 = \sqrt{|\delta^2 - \Gamma^2|}$. The symmetry breaking occurs at the exceptional points (EPs) $|\delta/\Gamma| = 1$, where the eigenstates coalesce, $\lambda_{\pm} = -i\frac{\kappa+\Gamma}{2}$. In the broken anti-PT phase $|\delta/\Gamma| > 1$, the two eigenvalues $\lambda_{\pm} = -i\frac{\kappa+\Gamma}{2} \pm \frac{1}{2}\lambda_0$ are complex. For the cavity decay rate $\kappa = 0$, there exists the singular point ($\delta = 0$) corresponding to the VIC induced zero linewidth (namely $\text{Im}\lambda_+ = 0$) in the anti-PT symmetric phase. The feature is essential for sensing of weak anharmonicities [18].

For $\Phi = 2n\pi + \phi$ with a finite phase deviation $\phi \neq 0$, the matrix \mathcal{H} becomes ϕ dependent. A weak coherent coupling with the amplitude $(\Gamma/2)\sin\Phi \sim \Gamma\phi/2$ for $\phi \ll \pi$ is introduced to the coupled cavity modes, and the anti-PT symmetry breaks down. The eigenvalues of the matrix \mathcal{H} now read

$$\lambda_{\pm} = -i\left(\frac{\kappa+\Gamma}{2} \mp \frac{\Gamma}{2}\tilde{\lambda}_0\cos\frac{\theta}{2}\right) \mp \frac{\Gamma}{2}\tilde{\lambda}_0\sin\frac{\theta}{2} \quad (20)$$

with

$$\tilde{\lambda}_0 = \left(1 + \frac{\delta^4}{\Gamma^4} - 2\frac{\delta^2}{\Gamma^2}\cos 2\Phi\right)^{\frac{1}{4}}, \quad (21)$$

$$\theta = \arctan\left(\frac{\Gamma^2\sin 2\Phi}{\Gamma^2\cos 2\Phi - \delta^2}\right). \quad (22)$$

Compared with the case of the completely dissipative coupling regime, both the real and imaginary parts of λ_{\pm} become nondegenerate and nonzero regardless of the value of δ , see the solid lines in Figs. 2(a)-(b). In other

words, there does not exist the EPs which strictly correspond to the degeneracy points in the spectra. In this case, we note that $\theta = 2\phi$ at $\delta = 0$, and thus $\text{Im}\lambda_+ \approx -\frac{1}{2}(\kappa + \frac{\Gamma}{2}\phi^2)$, as indicated by the arrow in Fig. 2(b). It implies that the system is now subject to a weak loss induced by the waveguide-mediated coherent coupling, namely, there does not exist the real singularity with a completely vanishing linewidth (i.e. the VIC induced zero linewidth) even though the cavity decay κ is set to zero. When the system is engineered to be anti-PT symmetric, a dissipative eigenmode may reduce the sensitivity for sensing of weak anharmonicity in the cavity modes [18]. However, the imaginary part of λ_+ remains negligible compared to Γ (i.e. $\text{Im}\lambda_+/\Gamma \sim 10^{-3}$), as the result of the coherence induced symmetry breaking, see the inset in Fig. 2(b). Indeed, we find that a weak coherent coupling $(\Gamma/2)\sin\phi$ still allows for a long-lived cavity resonance, and remarkably, it can induce optical bistability around the cavity resonance at weak cavity driving power, which can not happen for the anti-PT symmetric Hamiltonian Eq. (18) with $\delta = 0$ [53]. By combining the linewidth suppression with the optical bistability, the sensitivity of detecting the OMIN can be greatly enhanced, and moreover, can be resistant to a finite inherent cavity linewidth, see the details in Sec. V.

IV. COHERENCE INDUCED BISTABILITY

To demonstrate enhanced sensing of the OMIN with the coupled cavity-waveguide system, we now include the optomechanical coupling term as a perturbative probe, and consider the classical Langevin equation of motions for the mean (steady-state) values of the field and mechanical operators $\alpha_j \equiv \langle \hat{a}_j \rangle$, $\langle \hat{q} \rangle$ and $\langle \hat{p} \rangle$ under the mean-field approximation $\langle \hat{q} \hat{a}_1 \rangle \approx \langle \hat{q} \rangle \langle \hat{a}_1 \rangle$ and $\langle \hat{a}_1^\dagger \hat{a}_1 \rangle \approx |\alpha_1|^2$. It follows that

$$\dot{\alpha}_1 = i\frac{\delta}{2}\alpha_1 - \frac{\kappa + \Gamma}{2}\alpha_1 - e^{i\Phi}\frac{\Gamma}{2}\alpha_2 - ig\langle \hat{q} \rangle \alpha_1 + \Omega, \quad (23)$$

$$\dot{\alpha}_2 = -i\frac{\delta}{2}\alpha_2 - \frac{\kappa + \Gamma}{2}\alpha_2 - e^{i\Phi}\frac{\Gamma}{2}\alpha_1, \quad (24)$$

$$\dot{\langle \hat{q} \rangle} = \omega_m \langle \hat{p} \rangle, \quad (25)$$

$$\dot{\langle \hat{p} \rangle} = -\omega_m \langle \hat{q} \rangle - g|\alpha_1|^2 - \gamma_m \langle \hat{p} \rangle. \quad (26)$$

In the steady state for Eqs. (23)-(26), i.e., $\dot{\alpha}_1 = \dot{\alpha}_2 = \dot{\langle \hat{q} \rangle} = \dot{\langle \hat{p} \rangle} = 0$, and by eliminating the mechanical degree of freedom, we find the modified relations for the field amplitudes

$$\left(-i\frac{\delta}{2} + \frac{\kappa + \Gamma}{2}\right)\alpha_1 + e^{i\Phi}\frac{\Gamma}{2}\alpha_2 - i\frac{g^2}{\omega_m}|\alpha_1|^2\alpha_1 = \Omega, \quad (27)$$

$$\alpha_2 = \frac{-\Gamma e^{i\Phi}}{i\delta + (\kappa + \Gamma)}\alpha_1. \quad (28)$$

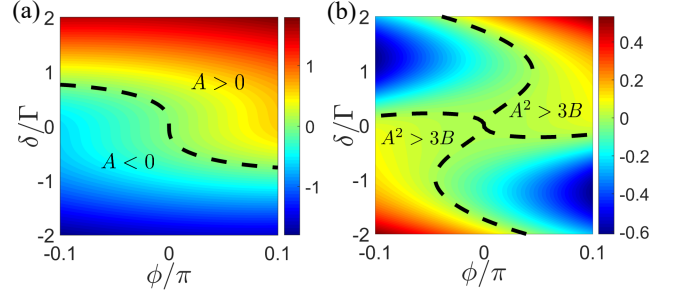


Figure 3. (Color online) The necessary conditions for bistability. (a) Dimensionless A/Γ and (b) $(A^2 - 3B)/\Gamma$ plotted against ϕ and δ . The black dashed lines indicate $A = 0$ in (a) and $A^2 = 3B$ in (b).

Moreover, by inserting Eq. (28) into Eq. (27), the cavity intensity $\beta \equiv |\alpha_1|^2$ is found to satisfy a cubic relation

$$\chi^2\beta^3 + \chi A\beta^2 + B\beta = I, \quad (29)$$

where $\chi = g^2/\omega_m$ is the Kerr-type nonlinearity induced by the optomechanical interaction, $I = \Omega^2$ is proportional to the input laser power P_{in} ,

$$A = \delta + \frac{\Gamma^2 [-\delta\cos 2\Phi + (\kappa + \Gamma)\sin 2\Phi]}{\delta^2 + (\kappa + \Gamma)^2} \quad (30)$$

and

$$B = \frac{\delta^2 + (\kappa + \Gamma)^2}{4} + \frac{1}{4} \frac{\Gamma^4}{\delta^2 + (\kappa + \Gamma)^2} - \frac{\Gamma^2}{2} \cos 2\Phi. \quad (31)$$

For the completely dissipative coupling regime $\Phi = 2n\pi$, Eq. (29) entails a bistable response to a strong driving I only when $|\delta| > \sqrt{3}(\kappa + \Gamma)$, namely, a bistability behavior can not be found in the anti-PT symmetry phase corresponding to $|\delta/\Gamma| < 1$. However, we find that a bistable response to both ϕ and δ can happen by including the weak coherent coupling $\sim \frac{\Gamma}{2}\sin\Phi$, at low driving power and small detuning $|\delta/\Gamma| \ll 1$. For the driving power dependence of the cavity intensity β , the bistability turning points can be derived from Eq. (29) by inspecting the solutions of $dI/d\beta = 0$, which turn out to be

$$\beta_{\pm} = \frac{-A \pm \sqrt{A^2 - 3B}}{3\chi}. \quad (32)$$

Thus, the necessary conditions for observing a bistable signature are $A < 0$ and $A^2 > 3B$, which are shown in Fig. 3 by plotting them against δ and ϕ . The boundaries $A = 0$ and $A^2 = 3B$ between the monostable and the bistable regions are indicated by the dashed lines. It can be seen that the bistable region embraces the small detuning regime $|\delta/\Gamma| \rightarrow 0$ for a finite negative phase $\phi < 0$, namely, the VIC induced linewidth suppression and the static optical bistability can co-exist.

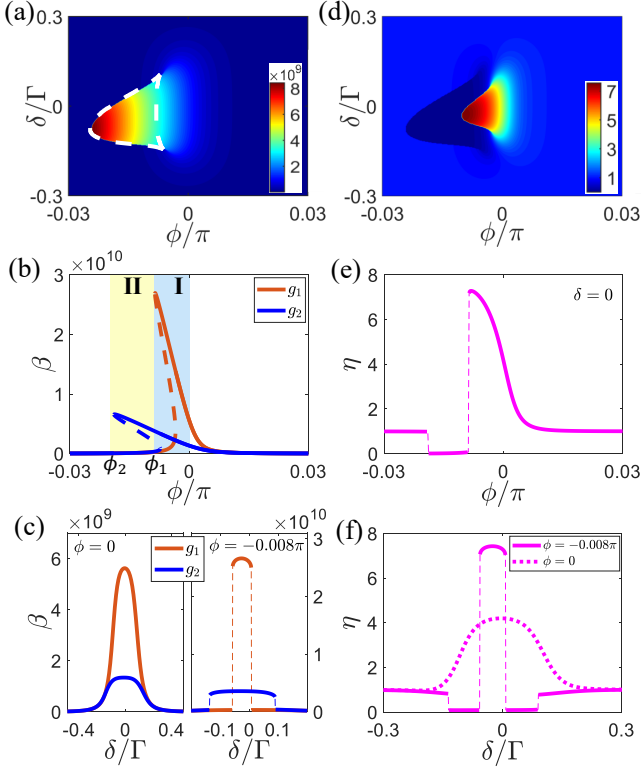


Figure 4. (Color online) (a) Cavity intensity β plotted against ϕ and δ for optomechanical coupling strength $g/2\pi = 3$ Hz. The white dashed line encircles the bistable region. (b) Cavity intensity β on resonance $\delta = 0$ versus ϕ for optomechanical coupling strengths $g_1/2\pi = 1$ Hz and $g_2/2\pi = 3$ Hz, respectively. ϕ_1 and ϕ_2 denote the upper turning points of the curves, which are the boundaries related to the two highlighted regions I and II. (c) Cavity intensity β versus δ/Γ with $\phi = 0$ (the left panel) and $\phi = -0.008\pi$ (the right panel). (d) The sensitivity factor η defined by Eq. (33) plotted against ϕ and δ . (e) η versus δ/Γ with $\phi = 0$, -0.008π . Other parameters are: $\Gamma/2\pi = 100$ MHz, $\omega_m/2\pi = 10$ kHz, $\kappa/\Gamma = 2 \times 10^{-3}$, $P_{\text{in}} = 8.06$ mW with $\lambda_d = 1550$ nm.

By combining the two effects, the response of the cavity intensity β to optomechanical interactions around $|\delta/\Gamma| \ll 1$ can be strong, which is important for the sensing scheme. However for $\phi > 0$, only a monostable behavior can be found.

V. SENSING OPTOMECHANICAL INTERACTION ENHANCED BY BISTABILITY

Since the weak single-photon optomechanical coupling g/ω_m is typically on the order ranging from 10^{-7} to 10^{-4} [52, 65–69], the optomechanical interaction induced Kerr nonlinearity $\chi = g^2/\omega_m$ can only be measured with a reasonably strong laser driving. Its effect is reflected in the response of the cavity intensity β of the cavity mode \hat{a}_1 . For the standard anti-PT symmetric system with $\phi = 0$ and $\kappa = 0$, the response to g

at $\delta = 0$ can be captured by the functional dependence $\beta \propto g^{-4/3}$ for $A = B = 0$, according to which the sensitivity to g is given by $|\delta\beta/\delta g| \propto g^{-7/3}$. Thus, a triple decrease in g (or approximately a tenfold decrease in χ) scales up the peak value of β by a factor of ~ 4 .

For $\phi \neq 0$, the response of β to g can be examined by solving Eq. (29), which may have one or two stable solutions. Here, β is plotted against the detuning δ and the phase deviation ϕ in Fig. 4(a) for the typical set of parameters: $g/2\pi = 3$ Hz, $\Gamma/2\pi = 100$ MHz, $\kappa/\Gamma = 2 \times 10^{-3}$, and $P_{\text{in}} \approx 8$ mW with $\lambda_d = 2\pi c/\omega_d = 1550$ nm [70, 71]. As expected, the bistability occurs only for negative ϕ . The asymmetry in the diagram with respect to ϕ arises from the fact that the stability condition Eq. (32) does depend on the sign of the coherent coupling strength $\frac{\Gamma}{2}\sin\phi$. Note that for weak cavity driving, the detuning and the weak coherent coupling associated with the bistable region, which is encircled by the white dashed line, are limited to $|\delta/\Gamma| < 0.14$ and $-0.012\Gamma < \frac{\Gamma}{2}\sin\phi < -0.003\Gamma$, respectively. We emphasize that the bistability does not exist for $\phi = 0$, corresponding to the case of the completely dissipative coupling regime.

For studying the sensitivity to g , we look into the modified bistability behavior of β by comparing its responses to two different optomechanical coupling strengths $g = g_1 = 2\pi \times 1$ Hz and $g = g_2 = 2\pi \times 3$ Hz. As shown in Fig. 4(b), we plot the cavity intensity β as a function of the phase deviation ϕ with $\delta = 0$ for $g = g_1$ and $g = g_2$, respectively. In both cases, β has two stable branches (solid) and one unstable branch (dashed). Recalling that the perfect anti-PT symmetric system relies on the fulfillment of the condition $\phi = 0$, here when ϕ is slowly swept backward, the cavity intensity β responds to the weak nonlinearity $\chi \propto g^2$ in a counter-intuitive way: the system shows bistability for both the optomechanical coupling strengths $g = g_1 = 2\pi \times 1$ Hz and $g = g_2 = 2\pi \times 3$ Hz, but the larger g (or the nonlinearity χ) is, the smaller peak value of the cavity intensity β has. For comparison with the anti-PT symmetric model, we show in Fig. 4(c) the cavity intensity β versus δ for $\phi = 0$ (the left panel) and $\phi = -0.008\pi$ (the right panel), corresponding to the monostable and bistable regimes, respectively. In both cases, β shows flat central peak around $\delta = 0$, benefiting from the VIC induced linewidth suppression. But for $\phi = -0.008\pi$, β has a peak value about four (two) times greater than that for $\phi = 0$ with $g = g_1$ ($g = g_2$). It proves that the optical bistability enables a stronger response of β to g .

Considering the sensing of the OMIN χ , there are generally two working regions [as highlighted in Fig. 4(b)], corresponding to $\phi \in (\phi_1, 0)$ (region I) and $\phi \in (\phi_2, \phi_1)$ (region II), respectively. Here ϕ_1 and ϕ_2 are the phase deviations corresponding to the turning points of the curves, where the upper branch starts from and the middle unstable branch ends. To be clear, we first define the sensitivity $\eta(\phi, \delta)$ as the ratio of the cavity intensities $\beta(g_1)$ and $\beta(g_2)$ at the *upper branches* with respect to the two optomechanical coupling strengths

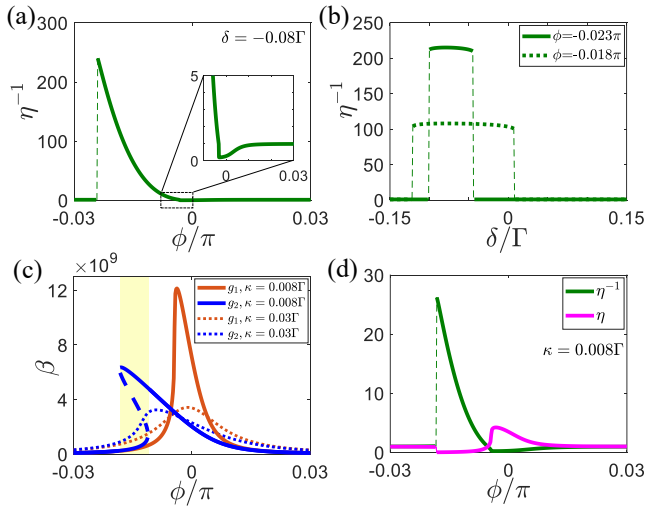


Figure 5. (Color online) (a) The sensitivity η^{-1} plotted against ϕ at $\delta = -0.08\Gamma$; (b) η^{-1} plotted against δ at $\phi = -0.018\pi, -0.023\pi$; (c) Cavity intensity β on resonance $\delta = 0$ versus ϕ for optomechanical coupling strengths $g_1/2\pi = 1$ Hz and $g_2/2\pi = 3$ Hz, where the cavity decay rates are set to $\kappa/\Gamma = 0.008$ and 0.03 . (d) The sensitivity factors η and η^{-1} versus ϕ on resonance $\delta = 0$ with $\kappa/\Gamma = 0.008$. Other parameters are the same as those in Fig. 4.

$g_1/2\pi = 1$ Hz and $g_2/2\pi = 3$ Hz, namely

$$\eta(\phi, \delta) = \frac{\beta(g_1)}{\beta(g_2)}, \quad (33)$$

which is appropriate for region I. While for region II, η^{-1} is used as the sensitivity instead. For an overview, we show $\eta(\phi, \delta)$ versus ϕ and δ in Fig. 4(d), where the red region corresponds to the enhanced sensitivity with the maximum $\eta_{\max} \sim 7.5$ for a triple decrease in g (i.e. $g_1/g_2 = 1/3$). In region I, for both coupling strengths the system displays monostability near $\phi = 0$ and optical bistability near $\phi = \phi_1$. The sensitivity $\eta(\phi, 0)$ at $\delta = 0$ is gradually increased for a backward sweep of the phase deviation from $\phi = 0.003\pi$ to $\phi = \phi_1 \approx -0.008\pi$, as shown in Fig. 4(e). It achieves the maximum $\eta(\phi_1, 0) \sim 7.3$, which is about twice that with $\phi = 0$. Moreover, a slight detuning allows for a better sensitivity for $\phi \approx -0.008\pi$, as manifested by the δ dependence of η shown in Fig. 4(f). The optimal $\eta(\phi = -0.008\pi, \delta)$ turns up at $\delta_{\text{opt}} \approx -0.025\Gamma$, and is resistant to a detuning deviation $\sim 0.03\Gamma$ from the optimal detuning δ_{opt} .

Next, we turn to region II in Fig. 4(b), where β becomes monostable for $g = g_1$ while maintains the bistability feature for $g = g_2$. In this regime, the sensitivity factor η approaches zero as ϕ sweeping backward and across ϕ_1 , but the inverse of it (as the new sensitivity factor) η^{-1} can be more than thirty times larger than the maximal η at region I. As shown in Fig. 5(a), we

plot η^{-1} as a function of ϕ with $\delta/\Gamma = -0.08$. Remarkably, η^{-1} increases from 0.3 to 240 in an almost monotonic manner when ϕ is swept backward from $\phi = 0$ to $\phi = \phi_2 = -0.024\pi$, except a weak dip at $\phi = -0.003\pi$ corresponding to the maximal $\beta(g_1)$. Furthermore, Fig. 5(b) shows that the high sensitivity (the maximum η^{-1}) remains flat within a certain frequency range, which can be referred to as the bandwidth for the measurement of the OMIN. Here the bandwidth is about 0.06Γ (0.13Γ) for $\phi = -0.023\pi$ ($\phi = -0.018\pi$). Therefore, the coupled cavity-waveguide system can act as a fluctuation-resistant and highly sensitive sensor.

Finally, we consider the effect of the cavity decay by increasing κ and meanwhile keeping the cavity driving power invariant. In Fig. 5(c), we show β as a function of ϕ with $\kappa/\Gamma = 8 \times 10^{-3}$ and $\kappa/\Gamma = 0.03$, respectively [72]. For $\kappa/\Gamma = 0.03$, the responses of β to $g_1/2\pi = 1$ Hz and $g_2/2\pi = 3$ Hz both show a strong quenching and become monostable. The intensities decrease sharply because a large cavity dissipation will inhibit the system from achieving long-lived resonance and amplitude accumulation. Since the profiles of the two dotted curves (with respect to $\kappa/\Gamma = 0.03$) are almost overlapped, the sensing scheme becomes invalid. While for a weaker inherent decay $\kappa/\Gamma = 8 \times 10^{-3}$, the behavior observed at region II [shown in Fig. 4(b)] replays, namely for $\phi \in (-0.018\pi, -0.011\pi)$, the response of β to $g_1/2\pi = 1$ Hz becomes monostable, while the response to $g_2/2\pi = 3$ Hz remains bistable [highlighted in Fig. 5(c)]. Thus, our model can still work as a high-performance sensor in this region and the sensitivity factor η^{-1} can still achieve a few tens. In comparison, the sensitivity η can only reach about 3 for the anti-PT symmetric model with respect to $\phi = 0$.

VI. DISCUSSIONS ON EXPERIMENTAL REALIZATION

To address the experimental feasibility, we consider an optomechanical setup with a levitated nanosphere [73–76], e.g. the silicon-vacancy (SiV) centers, coupling to the evanescent field of a microsphere cavity with frequency ω_c [54]. The dielectric nanosphere with a nanodiamond structure contains N two-level quantum emitters, which are driven by a bichromatic field of frequencies symmetrically red- and blue-detuned from the atomic transition frequency ω_0 , forming an optical trap for the nanosphere at a distance z from the cavity surface [54]. The emitter-cavity coupling $\Omega_c(\hat{z})$ then depends on the mechanical displacement of the nanosphere along the z axis, with the mechanical eigenfrequency ω_m . In the dispersive interaction regime, where the emitter-cavity detuning $\Delta_c \equiv \omega_c - \omega_0$ is much larger than Ω_c , and by considering that the induced atomic level Stark shift is much less than the excited-state linewidth, one can finally obtain the effective optomechanical interaction $\hat{H}_{\text{om}} = g\hat{a}^\dagger\hat{a}\hat{q}_z$ between the cavity

field and the mechanical motion, where [54]

$$g = -\sqrt{2}N(2p_e - 1)\frac{\Omega_c^2(z)}{2\Delta_c}\gamma_c q_{zpf} \quad (34)$$

is the single-photon coupling strength due to N quantum emitters, p_e is the steady excited-state population, \hat{q}_z is the mechanical displacement operator along the z axis from the equilibrium position with q_{zpf} the zero-point motion, and γ_c is the decay rate of the cavity's evanescent field, see Ref. [54] for the details.

The sensing device can then build on an optomechanical cavity-waveguide system with two microcavities [32, 72, 77, 78], one of which couples to an optically trapped nanosphere. For the typical parameters [54]: $p_e \approx 3.2 \times 10^{-5}$, the density of quantum emitters $\rho_q \approx 1.4 \text{ nm}^{-3}$, the radius of the nanosphere $R = 15 \text{ nm}$, the mechanical frequency $\omega_m/2\pi \sim 10 \text{ kHz}$, and $\gamma_c^{-1} = 283 \text{ nm}$, one obtains the single-photon coupling strength $g/2\pi \sim 1 \text{ Hz}$ (or $\chi/2\pi \sim 100 \text{ }\mu\text{Hz}$) with the distance between the nanosphere and the cavity surface being $z = 783 \text{ nm}$. Moreover, the inherent decay rate for the microcavity is typically $\kappa/2\pi \sim 10 \text{ kHz}$, which is much less than the waveguide induced coupling ($\sim 100 \text{ MHz}$) between the cavity modes [71]. Therefore, the coupled cavity-waveguide device can in principle be used for sensing weak perturbations on the set of parameters with respect to the optomechanical interaction and the induced Kerr nonlinearity.

VII. CONCLUSION

In summary, we have studied the sensitivity enhancement for measuring the OMIN with two cavities coupled via a vacuum optical waveguide. When the phase accumulation of light propagation from one cavity to

the other is precisely a multiple of 2π , the two cavities are dissipatively coupled. In this regime, the system can be anti-PT symmetric, and its Hamiltonian shows a singular point around the cavity resonance ($\delta = 0$), corresponding to the VIC induced zero linewidth. This singularity has been exploited for sensing of a weak Kerr nonlinearity [18], but can be fragile to a nonzero coherent coupling and a finite cavity decay rate. In addition, the standard anti-PT symmetric system shows bistability only at the broken anti-PT phase with $|\delta/\Gamma| > 1$ [53]. Although the standard anti-PT symmetry cannot be held when a small phase deviation is introduced, we find that both the VIC induced linewidth suppression and optical bistability can be observed around the cavity resonance $\delta/\Gamma \sim 0$. The joint effect allows us to greatly enhance the sensitivity for measuring the OMIN, which can reach a few hundreds for a triple reduction of the single-photon optomechanical coupling strength. The high sensitivity can be retained for a bandwidth of a few megahertz, and can remain a few tens for a cavity decay rate of hundreds of kHz. While we consider the setup consisting of an optically levitated nanodiamond coupled to waveguide-coupled microspheres [54], the model can be generalized to other integrated optomechanical cavity-waveguide systems, such as hybrid cavity-magnonic systems [55, 56], optomechanical crystal circuits [57], and microwave optomechanical circuits [58].

ACKNOWLEDGMENTS

H.W. acknowledges support from the National Natural Science Foundation of China (NSFC) under Grants No. 11774058 and No. 12174058. Y.L. acknowledges support from the NSFC under Grants No. 12074030 and No. 12274107.

-
- [1] C. L. Degen, F. Reinhard, and P. Cappellaro, *Rev. Mod. Phys.* **89**, 035002 (2017).
 - [2] M. Brownnutt, M. Kumph, P. Rabl, and R. Blatt, *Rev. Mod. Phys.* **87**, 1419 (2015).
 - [3] K. Jensen, R. Budvytyte, R. A. Thomas, T. Wang, A. M. Fuchs, M. V. Balabas, G. Vasilakis, L. D. Mosgaard, H. C. Stærkind, J. H. Muller, T. Heimburg, S. P. Olesen, and E. S. Polzik, *Sci. Rep.* **6**, 29638 (2016).
 - [4] S. Schmitt, T. Gefen, F. M. Stürner, T. Unden, G. Wolff, C. Müller, J. Scheuer, B. Naydenov, M. Markham, S. Pezzagna, J. Meijer, I. Schwarz, M. Plenio, A. Retzker, L. P. McGuinness, and F. Jelezko, *Science* **356**, 832 (2017).
 - [5] J. Moser, J. Güttinger, A. Eichler, M. J. Esplandiu, D. E. Liu, M. I. Dykman, and A. Bachtold, *Nature Nanotech.* **8**, 493 (2013).
 - [6] A. G. Krause, M. Winger, T. D. Blasius, Q. Lin, and O. Painter, *Nat. Photonics* **6**, 768 (2012).
 - [7] E. Gil-Santos, D. Ramos, J. Martínez, M. Fernández-Regúlez, R. García, Á. San Paulo, M. Calleja, and J. Tamayo, *Nature Nanotech.* **5**, 641 (2010).
 - [8] J. Wiersig, *Phys. Rev. Lett.* **112**, 203901 (2014).
 - [9] L. Chang, X. Jiang, S. Hua, C. Yang, J. Wen, L. Jiang, G. Li, G. Wang, and M. Xiao, *Nat. Photonics* **8**, 524 (2014).
 - [10] Z. Xiao, H. Li, T. Kottos, and A. Alù, *Phys. Rev. Lett.* **123**, 213901 (2019).
 - [11] B. Dóra, D. Sticlet, and C. P. Moca, *Phys. Rev. Lett.* **128**, 146804 (2021).
 - [12] I. Katsantonis, S. Droulias, C. M. Soukoulis, E. N. Economou, T. P. Rakitzis, and M. Kafesaki, *Phys. Rev. B* **105**, 174112 (2022).
 - [13] L. Ge and H. E. Türeci, *Phys. Rev. A* **88**, 053810 (2013).
 - [14] J. Wang, D. Mukhopadhyay, and G. S. Agarwal, *Phys. Rev. Research* **4**, 013131 (2022).
 - [15] X.-W. Luo, C. Zhang, and S. Du, *Phys. Rev. Lett.* **128**, 173602 (2022).
 - [16] S. Park, D. Lee, K. Park, H. Shin, Y. Choi, and J. W. Yoon, *Phys. Rev. Lett.* **127**, 83601 (2021).

- [17] H. Zhang, R. Huang, S. D. Zhang, Y. Li, C. W. Qiu, F. Nori, and H. Jing, *Nano Lett.* **20**, 7594 (2020).
- [18] J. M. Nair, D. Mukhopadhyay, and G. S. Agarwal, *Phys. Rev. Lett.* **126**, 180401 (2021).
- [19] W. Chen, S. Kaya Özdemir, G. Zhao, J. Wiersig, and L. Yang, *Nature (London)* **548**, 192 (2017).
- [20] H. Hodaei, A. U. Hassan, S. Wittek, H. Garcia-Gracia, R. El-Ganainy, D. N. Christodoulides, and M. Khajavikhan, *Nature (London)* **548**, 187 (2017).
- [21] R. El-Ganainy, K. G. Makris, M. Khajavikhan, Z. H. Musslimani, S. Rotter, and D. N. Christodoulides, *Nat. Phys.* **14**, 11 (2018).
- [22] M. A. Miri and A. Alù, *Science* **363**, 7709 (2019).
- [23] H. Li, A. Mekawy, A. Krasnok, and A. Alù, *Phys. Rev. Lett.* **124**, 193901 (2020).
- [24] Y. Yang, Y. P. Wang, J. W. Rao, Y. S. Gui, B. M. Yao, W. Lu, and C. M. Hu, *Phys. Rev. Lett.* **125**, 147202 (2020).
- [25] P. Peng, W. Cao, C. Shen, W. Qu, J. Wen, L. Jiang, and Y. Xiao, *Nat. Phys.* **12**, 1139 (2016).
- [26] X. Yin and X. Zhang, *Nat. Mater.* **12**, 175 (2013).
- [27] L. Feng, M. Ayache, J. Huang, Y.-L. Xu, M.-H. Lu, Y.-F. Chen, Y. Fainman, and A. Scherer, *Science* **333**, 729 (2011).
- [28] L. Feng, Z. J. Wong, R. M. Ma, Y. Wang, and X. Zhang, *Science* **346**, 972 (2014).
- [29] H. Hodaei, M. A. Miri, M. Heinrich, D. N. Christodoulides, and M. Khajavikhan, *Science* **346**, 975 (2014).
- [30] J. W. Yoon, Y. Choi, C. Hahn, G. Kim, S. H. Song, K.-Y. Yang, J. Y. Lee, Y. Kim, C. S. Lee, J. K. Shin, H.-S. Lee, and P. Berini, *Nature (London)* **562**, 86 (2018).
- [31] X. L. Zhang, T. Jiang, and C. T. Chan, *Light: Sci. Appl.* **8**, 88 (2019).
- [32] T. C. Chen and M. C. M. Lee, *J. Lightw. Technol.* **36**, 2966 (2018).
- [33] Z. Dong, Z. Li, F. Yang, C.-W. Qiu, and J. S. Ho, *Nat. Electron.* **2**, 335 (2019).
- [34] Y. Choi, C. Hahn, J. W. Yoon, and S. H. Song, *Nat. Commun.* **9**, 2182 (2018).
- [35] E. Paspalakis and P. L. Knight, *Phys. Rev. Lett.* **81**, 293 (1998).
- [36] C. H. Keitel, *Phys. Rev. Lett.* **83**, 1307 (1999).
- [37] G. S. Agarwal, *Phys. Rev. Lett.* **84**, 5500 (2000).
- [38] M. O. Scully, *Phys. Rev. Lett.* **104**, 207701 (2010).
- [39] K. P. Heeg, H. C. Wille, K. Schlage, T. Guryeva, D. Schumacher, I. Uschmann, K. S. Schulze, B. Marx, T. Kämpfer, G. G. Paulus, R. Röhlsberger, and J. Evers, *Phys. Rev. Lett.* **111**, 073601 (2013).
- [40] P. K. Jha, X. Ni, C. Wu, Y. Wang, and X. Zhang, *Phys. Rev. Lett.* **115**, 025501 (2015).
- [41] R. Hisatomi, A. Osada, Y. Tabuchi, T. Ishikawa, A. Noguchi, R. Yamazaki, K. Usami, and Y. Nakamura, *Phys. Rev. B* **93**, 174427 (2016).
- [42] V. V. Konotop and D. A. Zezyulin, *Phys. Rev. Lett.* **120**, 123902 (2018), 1802.07674.
- [43] D. Mukhopadhyay, J. M. Nair, and G. S. Agarwal, *Phys. Rev. B* **105**, 064405 (2022).
- [44] A. Bergman, R. Duggan, K. Sharma, M. Tur, A. Zadok, and A. Alù, *Nat. Commun.* **12**, 486 (2021).
- [45] D. A. Antonosyan, A. S. Solntsev, and A. A. Sukhorukov, *Opt. Lett.* **40**, 4575 (2015).
- [46] W. Li, Y. Zhou, P. Han, X. Chang, S. Jiang, A. Huang, H. Zhang, and Z. Xiao, *Phys. Rev. A* **104**, 033505 (2021).
- [47] A. Blais, A. L. Grimsmo, S. M. Girvin, and A. Wallraff, *Rev. Mod. Phys.* **93**, 25005 (2021).
- [48] H. Gothe, T. Valenzuela, M. Cristiani, and J. Eschner, *Phys. Rev. A* **99**, 013849 (2019).
- [49] P. Z. Fonseca, E. B. Aranas, J. Millen, T. S. Monteiro, and P. F. Barker, *Phys. Rev. Lett.* **117**, 173602 (2016).
- [50] Y. Zheng, L. M. Zhou, Y. Dong, C. W. Qiu, X. D. Chen, G. C. Guo, and F. W. Sun, *Phys. Rev. Lett.* **124**, 223603 (2020).
- [51] I. Katz, A. Retzker, R. Straub, and R. Lifshitz, *Phys. Rev. Lett.* **99**, 040404 (2007).
- [52] M. Aspelmeyer, T. J. Kippenberg, and F. Marquardt, *Rev. Mod. Phys.* **86**, 1391 (2013).
- [53] J. M. P. Nair, D. Mukhopadhyay, and G. S. Agarwal, *Phys. Rev. B* **103**, 224401 (2021).
- [54] M. L. Juan, G. Molina-Terriza, T. Volz, and O. Romero-Isart, *Phys. Rev. A* **94**, 023841 (2016).
- [55] M. Harder, Y. Yang, B. M. Yao, C. H. Yu, J. W. Rao, Y. S. Gui, R. L. Stamps, and C. M. Hu, *Phys. Rev. Lett.* **121**, 137203 (2018).
- [56] B. Zare Rameshti and G. E. Bauer, *Phys. Rev. B* **97**, 014419 (2018).
- [57] K. Fang, M. H. Matheny, X. Luan, and O. Painter, *Nat. Photonics* **10**, 489 (2016).
- [58] N. R. Bernier, L. D. Tóth, A. K. Feofanov, and T. J. Kippenberg, *Phys. Rev. A* **98**, 023841 (2018).
- [59] A. Metelmann and A. A. Clerk, *Phys. Rev. X* **5**, 021025 (2015).
- [60] D. E. Chang, A. H. Safavi-Naeini, M. Hafezi, and O. Painter, *New J. Phys.* **13**, 023003 (2011).
- [61] Z. Wang, L. Du, Y. Li, and Y. X. Liu, *Phys. Rev. A* **100**, 053809 (2019).
- [62] L. Du, Y. T. Chen, and Y. Li, *Phys. Rev. Research* **3**, 043226 (2021).
- [63] Y. F. Xiao, M. Li, Y. C. Liu, Y. Li, X. Sun, and Q. Gong, *Phys. Rev. A* **82**, 065804 (2010).
- [64] L. Du, Z. Wang, and Y. Li, *Opt. Express* **29**, 3038 (2021).
- [65] O. Arcizet, P. F. Cohadon, T. Briant, M. Pinard, A. Heidmann, J. M. MacKowski, C. Michel, L. Pinard, O. Français, and L. Rousseau, *Phys. Rev. Lett.* **97**, 133601 (2006).
- [66] S. Gröblacher, J. B. Hertzberg, M. R. Vanner, G. D. Cole, S. Gigan, K. C. Schwab, and M. Aspelmeyer, *Nat. Phys.* **5**, 485 (2009).
- [67] S. Gröblacher, K. Hammerer, M. R. Vanner, and M. Aspelmeyer, *Nature (London)* **460**, 724 (2009).
- [68] D. Kleckner, B. Pepper, E. Jeffrey, P. Sonin, S. M. Thon, and D. Bouwmeester, *Opt. Express* **19**, 19708 (2011).
- [69] T. Rocheleau, T. Ndukum, C. MacKlin, J. B. Hertzberg, A. A. Clerk, and K. C. Schwab, *Nature (London)* **463**, 72 (2010).
- [70] T. Shi and S. Fan, *Phys. Rev. A* **87**, 063818 (2013).
- [71] B. Dayan, a. S. Parkins, T. Aoki, E. P. Ostby, K. J. Vahala, and H. J. Kimble, *Science* **319**, 22 (2008).
- [72] H. Takashima, K. Kitajima, Y. Tanaka, H. Fujiwara, and K. Sasaki, *Phys. Rev. A* **89**, 021801 (2014).
- [73] L. P. Neukirch, J. Gieseler, R. Quidant, L. Novotny, and A. Nick Vamivakas, *Opt. Lett.* **38**, 2976 (2013).
- [74] L. P. Neukirch, E. von Haartman, J. M. Rosenholm, and A. Nick Vamivakas, *Nat. Photonics* **9**, 653 (2015).
- [75] T. M. Hoang, J. Ahn, J. Bang, and T. Li, *Nat. Commun.* **7**, 12250 (2016).

- [76] D. E. Chang, C. A. Regal, S. B. Papp, D. J. Wilson, J. Ye, O. Painter, H. J. Kimble, and P. Zoller, Proc. Natl. Acad. Sci. USA **107**, 1005 (2010).
- [77] D. Farnesi, S. Pelli, S. Soria, G. Nunzi Conti, X. Le Roux, M. Montesinos Ballester, L. Vivien, P. Cheben, and C. Alonso-Ramos, Optica **8**, 1511 (2021).
- [78] S. M. Spillane, T. J. Kippenberg, O. J. Painter, and K. J. Vahala, Phys. Rev. Lett. **91**, 043902 (2003).